Wide Bandgap Perovskite Photovoltaic Cells for Stray Light Recycling in a System Emitting Broadband Polarized Light

Guillermo Martínez-Denegri,* Catarina G. Ferreira, Marco A. Ruiz-Preciado, Paul Fassl, Mariia Kramarenko, Ulrich W. Paetzold and Jordi Martorell*

Perovskite based photovoltaic (PV) cells are unique in combining low open-circuit voltage losses with a broad bandgap tunability. This makes them an ideal PV cell to recycle photons back into electrical power in a variety of illumination systems or light emitting devices. Here, advantage of these features is taken and wide bandgap (WBG) perovskite PV cells are incorporated in devices suitable for display illumination and demonstrate a high yield in stray light recycling back into electricity with up to a 37.5% power conversion efficiency. The specific device considered is a modified half-cylinder photonic plate designed to emit diffused broadband polarized light using a nonabsorbing reflective polarizer based on a random dielectric layer distribution. It is experimentally demonstrated that light recycling using appropriately tuned WBG perovskite PV cells becomes very efficient when implemented in systems where the light is emitted from narrowband sources, even if the emission spans a broad wavelength range.

1. Introduction

Optimizing the energy efficiency in illumination or opto-electronic light emitting devices such as displays is not only about improving the power to light conversion efficiency but also about reducing parasitic optical losses and recycling stray light. To reduce energy waste to a minimum, any light selective process within the specific device considered should rely on nondissipative mechanisms, while any stray or discarded light should be either reused or recycled back into electricity. A prominent example where such adequate light management to save energy is needed are liquid crystal displays (LCDs) where the process to obtain the required polarized light may result in significant light losses. Various optical structures for effective broadband reflective light polarization have been proposed

in the past, partially avoiding the use of light absorbing polarizing elements.[1,2] However, the most effective structures to obtain polarized light rely on hundreds of nanolayers or subwavelength gratings and to reuse the stray light, its polarization is changed applying mechanisms of limited efficiency.[3–6] Alternative approaches consider the recycling of unused light into electricity. Systems that combine light polarization with light harvesting using organic photovoltaic (PV) cells have been proposed but their energy-saving potential would be too small to be worthily employed.[7,8] Menéndez-Velázquez et al. proposed the application of polarizing re-emitting dyes and silicon PV cells,[9] but no PV analysis for the light recycling process was performed.

Perovskite based PV cells exhibit the optimal characteristics to efficiently recycle light in optoelectronic devices using visible light sources. They exhibit high power conversion efficiencies (PCEs) and low recombination losses, providing a high efficiency in the energy transfer process.[10–15] Moreover, their bandgap energy (E_g) can be widely tuned by engineering the perovskite composition, which promises a high level of adaptability to different specific applications.[16–23] In a previous study,[24] we proposed the design of a novel light guiding plate which would emit polarized light, while the light with the unwanted polarization could be recycled back into electricity by two perovskite PV cells placed at the front and back ends of the guide. A homogeneous diffused light emission was demonstrated as a result of the ergodic light propagation occurring in what was termed as a half-cylinder photonic plate (h-CPP).[25] It was conceptually demonstrated

G. Martínez-Denegri, C. G. Ferreira, M. Kramarenko, J. Martorell
ICFO–Institut de Ciències Fotòniques
The Barcelona Institute of Science and Technology
Castelldefels, Barcelona 08860, Spain
E-mail: guillermo.martinez-denegri@alumni.icfo.eu; jordi.martorell@icfo.es

M. A. Ruiz-Preciado, P. Fassl, U. W. Paetzold
Institute of Microstructure Technology
Karlsruhe Institute of Technology
Hermann-von Helmholtz-Platz 1, 76344 Eggenstein-Leopoldshafen,
Germany

M. A. Ruiz-Preciado, P. Fassl, U. W. Paetzold
Light Technology Institute
Karlsruhe Institute of Technology
Engesserstrasse 13, 76131 Karlsruhe, Germany

J. Martorell
Departament de Física
Universitat Politècnica de Catalunya
Terrassa 08222, Spain

ADVANCED
SCIENCE NEWS

www.advancedsciencenews.com

ADVANCED
ENERGY
MATERIALS

www.advenergymat.de

that a multilayer reflective polarizing structure deposited on top of such a h-CPP could be used to select the p-polarized light for transmission while reflecting the remaining light. Therefore, the s-polarized light would remain trapped in the guide and most of the p-polarized light would exit it after a given number of incidences on the polarizing structure. Provided the extremely low light absorption losses of an optimized design, it has been shown that almost all the trapped light, mostly s-polarized, is guided toward the perovskite PV cells.

2. Concept and Design

Herein, we experimentally implement a modified h-CPP emitting diffused polarized light for homogenous illumination and study its capability to effectively recycle unused light back to electricity by incorporating perovskite PV cells. The light guiding element we implemented relies on a unique combination of order and randomness to achieve ergodicity and broadband light polarization. More specifically, an h-CPP is employed to achieve ergodic light propagation, which is ideal to obtain a homogeneous light diffusion, and a multilayer reflective polarizer with randomly distributed layer thicknesses is used for broadband light polarization. As demonstrated in our previous study,[24] the randomness in the multilayer structure is key to achieve a low polarization extinction ratio of ≈0.1 for a broad range spanning the blue, green, and red spectra.

The actual implementation of the reflective polarizer on a curved surface employing standard thin-film deposition techniques may lead to nonuniform thickness of the layers.[26–29] Therefore, a structural analysis of the actual thickness profile on the specific geometry must be performed prior to the fabrication of the final multilayer structure. We parameterized the thickness profile of the multilayer obtained on the h-CPP when using magnetron sputtering to introduce it in the optical model employed for the multilayer design. The model provides a powerful combination of ray optics, a transfer matrix formalism, and an optimization algorithm to numerically compute the optimal layer thicknesses by an inverse design approach as described in ref. [24]. In addition, to account for possible experimental thickness deviations, we monitored the thickness of the different layers while the structure was being fabricated and always recalculated the optimal thickness for the following layers to obtain the lowest possible polarization extinction ratios. The result is a reflective structure that polarizes light for a broad range of angles and the required wavelengths to emit white light. To recycle the nontransmitted light, we fabricated and studied the performance of two kind of perovskite PV cells with E_g of ≈1.55 eV and ≈1.73 eV, respectively. The PV performance under device relevant conditions was measured and PCEs considerably above those obtained under air-mass global standard spectrum (AM1.5G) illumination were obtained. Finally, an optical setup was mounted to demonstrate light recycling while polarization selectivity is performed in an ensemble integrating the polarizing structure and a perovskite PV cell.

3. Results and Discussion

To study the effect of the h-CPP geometry on the films deposited by magnetron sputtering, a modified h-CPP was fabricated by depositing on the h-CPP surface a multilayer made of TiO_2 and SiO_2 alternated films, and its thickness profile was measured. As shown in **Figure 1**a, although all areas of the surface are covered, the films thicknesses are reduced in the vicinity, i.e., the intersection, of two adjacent half-cylinders. For instance, on the highest point of the half-cylinder in Figure 1a, a thickness of ≈2.49 µm was measured, whereas at the intersection between two of them, the film thickness is reduced to ≈1.62 µm. Therefore, to obtain the profile of the actual thicknesses, we linearly fitted the measured thickness of the multilayer at different points of a half-cylinder as a function of its azimuthal angle, in relation to the thickness from layers grown on a flat surface (nominal thickness). Such a fitting resulted in Equation (S1) from the Supporting Information and was applied to estimate the deposited thickness on any point of the h-CPP. Afterward, the inverse integration model was used to numerically compute the optimal multilayer structure to minimize the polarization extinction ratio taking into consideration the specific deposition profile analyzed above. The optimized structure was fabricated both on top of a flat glass substrate and on top of a h-CPP. The flat sample was used to characterize the deposited layers by measuring their thicknesses using spectroscopic ellipsometry. Moreover, the s- and p-polarization transmittance (Ts and Tp, respectively) were measured at three different angles of incidence, which agreed with the corresponding simulation, as described in Figure S1 in the Supporting Information. The independent optical characterization was used to confirm that the thicknesses of the different layers were correctly fitted with the ellipsometry spectra. Such a characterization procedure was also performed to reoptimize the multilayer during fabrication and to compensate for any thickness deviation after the deposition of some of the layers. The nominal thickness obtained is summarized in Table S1 in the Supporting Information, while the actual thickness on a half-cylinder surface point can be calculated from Equation (S1) in the Supporting Information. As presented in Table S1 in the Supporting Information and shown in the cross-section image of the structure in Figure 1b, a nonperiodic thickness distribution of the 25 layers was required in order to obtain an effective broadband polarized light transmission.

To analyze the optical performance of the fabricated polarizing structure, we measured its total spectral Ts and Tp when light was introduced perpendicularly through the flat surface of the h-CPP, employing the setup depicted in Figure S2 in the Supporting Information. In the configuration under study, p-polarized light corresponds to the light whose electric field component is contained on the plane of incidence, corresponding to the plane of the cross section shown in Figure 1a. The electric field of the s-polarized light is perpendicular to that same plane. The measured total Ts and Tp as a function of the wavelength are shown in Figure 1c. Firstly, Ts is below 5% for the red and green wavelengths of interest and below 10% for the blue one, which confirms the high reflectivity for s-polarized light by the fabricated multilayer structure. Secondly, Tp was ≈20% higher than Ts for such wavelengths, providing an effective reflective polarization of the incident light for such a range of wavelengths. The nonabsorptive polarization discrimination is achieved by the multilayer designed to combine Brewster's angle transmission for the p-polarized light with
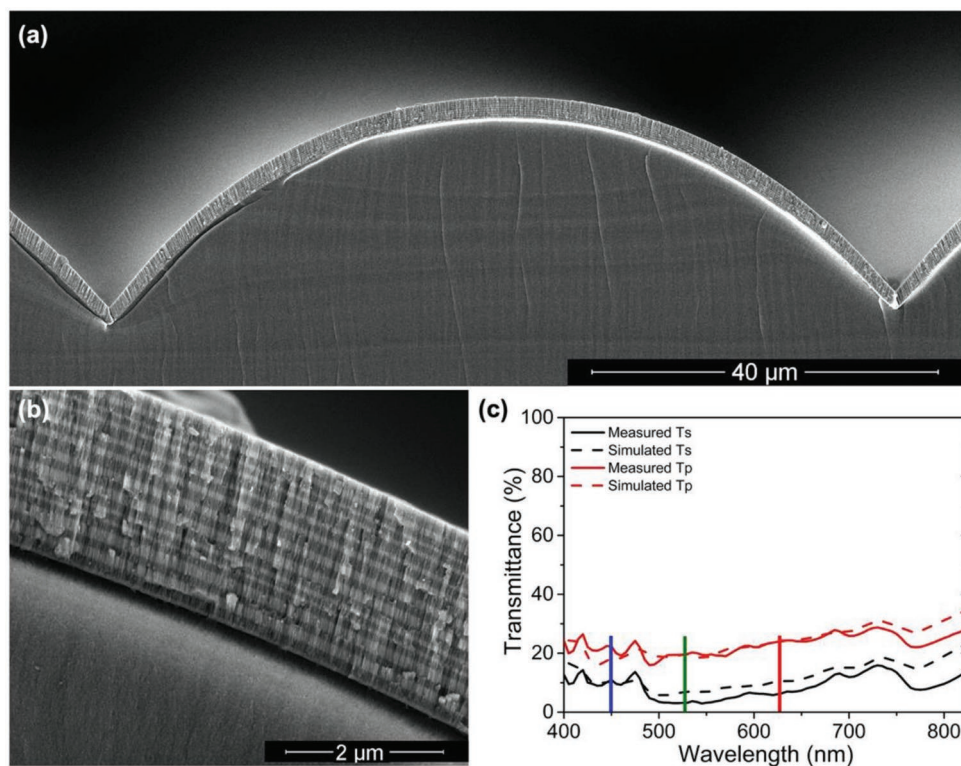
**ADVANCED
SCIENCE NEWS**

www.advancedsciencenews.com

**ADVANCED
ENERGY
MATERIALS**

www.advenergymat.de

Figure 1. Modified h-CPP. a) Scanning electron microscope (SEM) image of the multilayer structure deposited on the h-CPP. b) Magnified SEM images of the 25 layers structure. The darker areas are conformed by SiO_2 layers and the lighter ones by TiO_2. The sample was cut manually and, prior to its characterization, covered with an 8 nm film of sputtered Au/Pd to avoid charge accumulation. c) Total Ts and Tp of the multilayer structure deposited on the h-CPP compared with its corresponding simulation. The colored bars indicate the wavelengths of interest.

reflectivity at many interfaces for the s-polarized light which is enhanced by electromagnetic interference.

To achieve an energetically efficient diffused polarized light emission, we employed perovskite PV cells as elements to recycle the nonemitted light back into electricity. In order to maximize the efficiency of the recycling process, the perovskite bandgap should be engineered such that the wavelengths of the light emitted by the actual light source is efficiently absorbed, while being as close to the perovskite bandgap as possible to minimize the thermalization losses.[30] LCDs commonly employ red-green-blue (RGB) light emitting diodes (LEDs) sources in which the longest wavelength lies in the red region of the electromagnetic spectrum (≈635 nm). Therefore, the bandgap of the perovskite absorber for the application reported in this work should be increased when compared to the best-performing perovskite PV cells that are used to convert the entire sunlight spectrum (that reaches the deep infrared) into electricity most efficiently.

In this study, we analyze the light recycling capabilities of perovskite PV cells employing two different perovskite compositions: i) a low bandgap (LBG) perovskite with $E_g \approx 1.55$ eV, which is frequently used for highest solar energy conversion,[31–34] and ii) a wide bandgap (WBG) perovskite with $E_g \approx 1.73$ eV that is typically rather used for tandem solar cell applications.[17] We employ p-i-n perovskite PV cells with a structure of indium-tin oxide (ITO)/ ([2-(9H-carbazol-9-yl) ethyl]phosphonic acid) (2PACz)/perovskite/C_{60}/bathocuproine (BCP)/Ag and apply a perovskite surface passivation treatment

to reduce the recombination losses,[34] thus allowing a high open-circuit voltage (V_{oc}). To better estimate the amount of LED light that could be recycled to electrical power by the two types of perovskite PV cells incorporated on the modified h-CPP, we studied their performance under monochromatic illumination. Their current density–voltage (J–V) curves were acquired for the three different wavelengths corresponding to the RGB emission: 635, 532, and 450 nm. The illumination intensity was set to 100 mW cm^{-2} which, besides being the standardized power density for sunlight irradiation on the Earth surface, it is also similar to the illumination intensity that the cells would receive in our light recycling design (cf. Figure S3, Supporting Information). The PV performance of the LBG and WBG perovskite PV cells under these conditions is reported in **Figure 2**a and **Table 1**, yielding PCEs of 25.4%, 29.2%, and 33.7% for LBG and 30.4%, 35%, and 37.5% for WBG, corresponding to red, green, and blue emission, respectively. Comparing the J–V curves with those obtained under AM1.5G irradiation (Figure S4, Supporting Information), it becomes clear that both perovskite PV devices exhibit a much higher PCE under RGB illumination. The main reason for this higher PCE is that, as shown in Figure 2b, the perovskite PV cells in the presented application exhibit a remarkably higher external quantum efficiency (EQE) at the monochromatic RGB wavelengths relative to the integrated EQE when the complete solar spectrum is considered, which leads to a higher short-circuit current density (J_{sc}). Note that the J_{sc} increases with increasing illumination wavelength

ADVANCED
SCIENCE NEWS
www.advancedsciencenews.com

ADVANCED
ENERGY
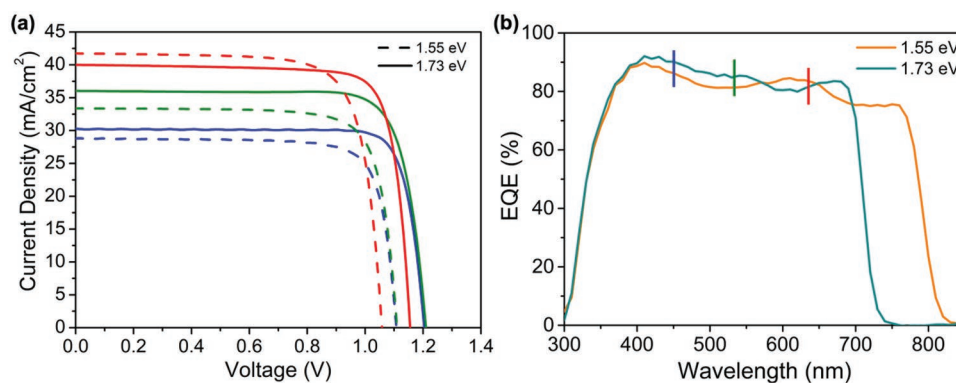**MATERIALS**
www.advenergymat.de

Figure 2. Perovskite PV cells performance. a) $J-V$ characteristics of the perovskite PV cells illuminated under the three monochromatic sources. The red, green, and blue colors represent whether the measurement has been performed with the 635, 532, or 450 nm monochromatic light source. The solid and dashed lines correspond to the WBG and LBG PSCs, respectively. b) EQE of the two types of perovskite PV cells. The colored bars indicate the points of the EQE spectra at the specific RGB wavelengths. The cell structure is glass/ITO/2PACz/$Cs_{0.18}FA_{0.82}Pb(I_{1-x}Br_x)_3$/C60/BCP/Ag, being $x = 0$ for the 1.55 eV and $x = 0.4$ for the 1.73 eV perovskite absorber, respectively.

which is due to the higher photon flux at lower wavelengths and equal illumination intensity. The exceptionally high J_{sc} obtained under monochromatic illumination, together with the high V_{oc} and fill factor (FF), leads to PCEs that more than doubles the one obtained when the illumination is the AM1.5G spectrum, as provided in Figure S4 in the Supporting Information. When comparing the results for the two types of perovskite PV cells investigated in more detail, the EQE of the WBG PV cell was relatively higher for the two shorter wavelengths, 450 and 532 nm, while for the 635 nm it was slightly lower, which explains the slight differences in J_{sc}. As expected, the largest difference is reflected in the V_{oc}, being about 100 mV higher for the WBG perovskite PV cell as compared the LBG one. To summarize, we obtained PCEs ranging from 30.4% to 37.5% for the WBG perovskite PV cell, approximately 5% higher than the PCE exhibited by the LBG one. Part of this higher PCE can be also attributed to the slightly improved FF for the WBG cells, which is even above 80%. It is worth highlighting that in our monochromatic illumination experiments the V_{oc} was underestimated provided the illuminated area of the PV cell was much smaller than the total area of the cell, which created a shadow effect.[35]

As a next step, to evaluate the light recycling capability of a configuration designed with the primary role to emit diffused polarized light, we combined the modified h-CPP and the perovskite PV cells. As shown in **Figure 3a**, a prism was attached to the h-CPP backside where the mirror was deposited. In this

way, s- and p-polarized green light was coupled into the guide by first polarizing the light coming from the source and measuring the $I-V$ curves of the PV cell for both types of light polarization separately. Additional details of the light propagation path are given in Section S2 in the Supporting Information. To overcome the large light coupling losses, we used a high-power green laser emitting at 532 nm. Enough power was applied to obtain an intensity at the end of the guide similar to the one that would be obtained from LED light optimally coupled as in standard LCD light guiding plates. Note that achieving an optimal light coupling is beyond the scope of this work. As can be seen in Figure 3b, the J_{sc} obtained by the perovskite PV cell from s-polarized light (≈ 37.6 mA cm^{-2}) is more than double that obtained from p-polarized light (≈ 17.4 mA cm^{-2}). Moreover, as summarized in **Table 2**, this larger current density does not imply a significant difference in the measured cell FF or V_{oc}. However, the V_{oc} obtained from the p-polarized illumination is slightly lower due to the lower intensity reaching the perovskite PV cell, considering that a large fraction of the p-polarized light is emitted through the cylindrically patterned surface of the modified h-CPP. The results reported in Figure 3b and Table 2 clearly demonstrate the light recycling capability of the WBG perovskite PV cell for systems where light absorbing elements, which in the end would lead to the dissipation of a large fraction of the input energy, are eliminated.

Employing a similar setup as the one shown in Figure 3a, we also measured the s-polarization and p-polarization current ratios (Is/Ip) delivered by the perovskite PV cell when red, green, and blue light from low power laser diodes was coupled into the guide (cf. **Table 3**). For the red and green wavelengths, the ratio is close to 2, clearly indicating that the s-polarized light at such wavelengths is more effectively trapped in the

Table 1. PV parameters of the LBG and WBG PSCs under monochromatic illumination at 100 mW cm^{-2}.

	Wavelength [nm]	J_{sc} [mA cm^{-2}]	V_{oc} [V]	FF [%]	PCE [%]
LBG (1.55 eV)	450	28.8	1.108	79.7	25.4
	532	33.4	1.110	78.7	29.2
	635	41.7	1.058	76.4	33.7
WBG (1.73 eV)	450	30.2	1.204	83.5	30.4
	532	36.0	1.210	80.2	35.0
	635	40.0	1.155	81.1	37.5

Table 2. PV parameters of the WBG PV cell measurement when s- and p-polarized light are inserted in the ensemble.

	J_{sc} [mA cm^{-2}]	V_{oc} [V]	FF [%]
s-polarization	37.6	1.216	79.4
p-polarization	17.4	1.188	79.8

ADVANCED
SCIENCE NEWS
www.advancedsciencenews.com

ADVANCED
ENERGY
MATERIALS
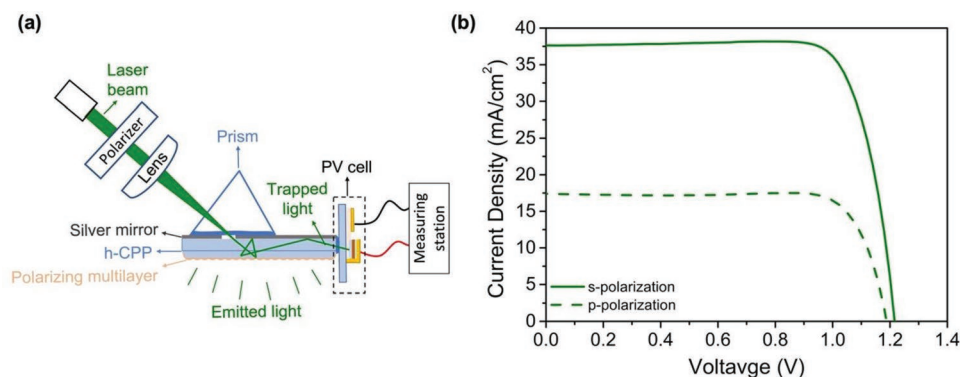www.advenergymat.de

Figure 3. Light recycling in the ensemble. a) Scheme of the ensemble with the different fabricated elements to measure the recycled nontransmitted light. The different elements were assembled employing an index matching fluid to ensure proper optical coupling. The drawing is not to scale. b) *J–V* curve of the WBG perovskite PV cell when introducing green light in the ensemble. Enough s-polarized light was introduced to obtain a similar current to direct illumination and, applying the same power, p-polarized light was inserted to characterize the ensemble under equal conditions for both polarizations. The small drift observed in the current density may be attributed to a slight instability of the laser power during the voltage scan measurement.

Table 3. Measured ratio of current generated from the different light polarization and simulated ratio of polarized light guided to the front end for the different wavelengths.

Wavelength [nm]	Measured Is/Ip[a]	Simulated s/p light on the front ends
450	1.67	3.03
532	1.96	2.00
635	2.19	2.57

[a]At least two different cells were measured under the different lights to ensure similar behavior.

guide than the p-polarized light. The measured current ratios agree well with the prediction from our model, the results of which are included in Table 3. A larger discrepancy between measurement and prediction is observed for the blue light case. Such a mismatch is originated from the fact that our numerical model computes the amount of s- and p-polarized light reaching the guide ends, but does not account for the light coupling effectiveness into the absorbing layer of the perovskite PV cell. As described in Section S3 in the Supporting Information, blue light coupling is strongly affected by the multilayer structure and absorption profile of the perovskite PV cell.

4. Conclusion and Future Work

To conclude, we have demonstrated the large potential of WBG perovskite PV cells to recycle unused or stray light back into electricity in display compatible optoelectronic illumination systems. The concept proposed herein prevents energy dissipation losses by almost completely eliminating any light absorbing element, other than the perovskite PV cells themselves. For WBG perovskite PV cells with a E_g of ≈1.73 eV, PCEs ranging from 30.5% to 37.5% were demonstrated under illumination using blue, green, and red monochromatic light sources, respectively. A PCE that more than doubles the one corresponding to AM1.5G illumination proves that light recycling using perovskite PV cells will become more effective when implemented in systems where the light is obtained from narrowband sources emitting in the visible spectrum, even if the

overall light emission spans a broad wavelength range. As a case study, we considered a modified h-CPP meant to emit diffused polarized light similarly to the light emission from the light guiding plates that are commonly used in LCDs. In the fabricated modified h-CPP, light polarization was achieved by a reflective polarizer based on a multilayer structure alternating high and low indexes of refraction. Instead of using a standard reflective polarizer with a periodic distribution of layers, we used an inverse design approach to obtain a random multilayer structure which can provide an optimal polarization extinction ratio at the three wavelengths from LED sources typically used for the illumination of LCD displays. The polarization extinction ratio as well as the transmitted p-pol light power achieved in the current h-CPP design, could be increased by the use of more uniform deposition methods such as atomic layer deposition or high-power pulsed magnetron sputtering.[36,37] In such scenario, the optimized polarizing structure applied for display illumination could reach a polarized light emission larger than 37% of the total incident light,[24] while the presented WBG perovskite PV cells would recycle the stray light with an average efficiency over 34%. Therefore, the combination of these elements could reduce the power losses relative to devices that incorporate absorbing polarizers by about 20%, as detailed in Section S4 in the Supporting Information. However, this is not the ultimate limit and light power losses may be reduced even more by a further optimization of the perovskite cell, the polarizing element and the h-CPP. Note that as opposed to other PV materials such as, for instance InGaP, the absorption band of the perovskite cells can be finely tuned to achieve the optimal match with the light emission bands of the LED sources. Given the novelty and the light recycling effect achieved, the completely novel light management approach from the current study may set the path for perovskite PV cell integration in many illumination or optoelectronic systems to enhance energy efficiency while preventing energy dissipation.

5. Experimental Section

Inverse Design for the Optimization of the Polarizing Multilayer Structure: To describe the light propagation in the modified h-CPP ray optics are

combined, for light propagation in the core of the h-CPP, with a full wave vector approach implemented using the transfer matrix method, for light propagation within the thin layers of the reflective polarizer. The optimal layer thicknesses for each layer of such polarizer were determined by an inverse design approach, using a genetic algorithm, in order to minimize the polarization extinction ratio (i.e., to maximize the ratio between the p- and s-polarized light transmitted out of the h-CPP) for three different wavelengths, corresponding to the blue (450 nm), green (532 nm), and red (635 nm) emission of LEDs. A more detailed explanation on the inverse design simulations can be found in ref. [24].

Modified h-CPP Fabrication and Characterization: The h-CPP was fabricated on a transparent polymer (OrmoComp, Micro Resist Technology GmbH) by drop casting it onto a metallic mold patterned with the negative periodic geometry. Then, a glass substrate was deposited on top of the liquid polymer and when the polymer had completely contacted the substrate surface it was cured under UV light for 5 min. The metallic mold was removed and the hardened polymer was exposed to UV light for 10 more minutes. The samples were then annealed to 135 °C on a hotplate for 10 min and placed on a vacuum oven at 150 °C for 3 h. The multilayer structure was fabricated on the h-CPP alternating TiO_2 and SiO_2 layers on the periodic surface of the h-CPP employing reactive magnetron sputtering. The TiO_2 layers were fabricated using a Ti target (Lesker, 99.97%) and DC power at 275 W in an atmosphere with a 4.5 sccm flux of O_2. The SiO_2 layers were deposited using a Si n-type target (Lesker, 99.999%) and radio-frequency power at 120 W in an atmosphere with a 2.16 sccm flux of O_2. All the processes were carried out at 3 mTorr of pressure and Ar as sputtering gas at 20 sccm. The deposited thickness was measured with a quartz balance and the shutter was closed when the nominal thickness was achieved. The optical characterization was carried out in a setup similar to the one presented in Figure S2 in the Supporting Information, which guides monochromatic light onto the aperture of an integrating sphere where the sample is placed so the light hit the sample on the flat surface. A polarizer was placed before the sample to polarize the incoming light. The nonabsorptive character of the multilayer was verified by measuring its reflectance and transmittance on a flat substrate at a given angle.

Optical Simulation of the Modified h-CPP: To simulate the light transmitted out of the h-CPP for each of the polarization components (Ts and Tp), a similar description for the light propagation, combining ray and wave optics, was considered. This time, however, the reflective element present on the bottom was eliminated and the light was incident from this surface instead of the lateral interface. Only few reflections of the light were considered in this case, as it quickly exits through one of the two fiber/air interfaces.

Perovskite PV Cells Fabrication: ITO substrates (sheet resistance 15 Ω sq^{-1}, Luminescence Technology) were cut in 30 mm × 30 mm and cleaned with acetone and isopropanol in an ultrasonic bath for 10 min each. The substrates were further treated with oxygen plasma for 3 min. As hole transporting layer, a monolayer of 2PACz was deposited on the ITO substrates by spin coating at 3000 rpm for 30 s and subsequently annealed at 100 °C for 10 min. The 2PACz precursor solution was prepared by dissolving 2PACz in anhydrous ethanol with a concentration of 1 mM. The prepared solution was put in an ultrasonic bath for 20 min before it was used. The LBG perovskite precursor solution was prepared by mixing PbI_2 (0.91 M), $PbBr_2$ (0.12 M), CsI (0.17 M), and formamidinium iodide (FAI) (0.83 M) in a mixture of dimethylformamide:dimethylsulphoxide (DMF:DMSO) (4:1 v/v). The WBG perovskite precursor solution was prepared by mixing PbI_2 (0.5 M), $PbBr_2$ (0.5 M), CsI (0.18 M), and FAI (0.83 M) in a mixture of DMF:DMSO (4:1 v/v). The perovskite films were spin coated on the substrates at 1000 rpm (200 rpm s^{-1}) for 10 s and 5000 rpm (2000 rpm s^{-1}) for 30 s. 15–20 s after the start of the second step, 200 µL chlorobenzene (for LBG perovskite) or ethyl acetate (for WBG perovskite) was quickly dropped in the center of the spinning substrate. The samples were then annealed at 150 °C (for LBG) or 100 °C (for WBG) for 30 min in a nitrogen atmosphere. For passivation, PEACl dissolved in 2-propanol (1.5 mg mL^{-1}) was dynamically spin coated at 5000 rpm on the perovskite films after cooling down and afterward annealed at 100 °C for 5 min. As the electron transport layer, 23 nm of

C_{60} and 3 nm BCP were thermally evaporated at a rate of 0.1–0.2 Å s^{-1} while maintaining a pressure not higher than 10^{-6} mbar. Finally, 100 nm of Ag was thermally evaporated using a shadow mask to complete the perovskite PV cells with 10 pixels per substrate with an active area of 24 mm^2. The area was confirmed measuring the contact electrode under an optical microscope. After the complete PV cells were fabricated, they were encapsulated with a cover glass using UV-curable OrmoComp resist (MicroResist Technology GmbH).

Perovskite PV Cells Characterization: The performance of the fabricated cells under sunlight was determined using an AM1.5G solar simulator (Sun 3000, Abet Technologies). The illumination intensity corresponding to 100 mW cm^{-2} was adjusted with a monocrystalline silicon reference cell (Hamamatsu, calibration October 2014) calibrated at the Fraunhofer Institute for Solar Energy Systems. The J–V curves were then recorded by scanning from 1.3 to −0.1 V using a Keithley 2400 SourceMeter and a scan speed of 350 mV s^{-1}. EQE analysis was performed using a quantum efficiency measurement system (QEX10, PV Measurements). In this case, the devices were illuminated using a monochromatic light coming from a xenon lamp. The spectral response of the calibrated silicon cell was used as a reference. The photovoltaic performance under monochromatic sources was carried out employing a red (CPS635R, Thorlabs), green (CPS532, Thorlabs), and blue (CPS450, Thorlabs) collimated laser diodes modules as light sources. The beam profile and the power emitted from each light source were previously measured and focused to illuminate the cells with 100 mW cm^{-2} for further measurement of the J–V curves. All the measurements were performed in air.

Setup and Characterization of the Integrated Ensemble: The ensemble was mounted joining the different element with an index matching fluid (NOA 150, Norland Products) as shown in Figure 3a. The modified h-CPP was contacted to a substrate with 150 nm of sputtered Ag deposited on it its backside, which conformed a light guide for the nontransmitted light. The Ag covered area had a slit of 2 mm to insert the light in the ensemble. A prism was attached to the silver layer in order to introduce tilted light avoiding partial reflection. Then, a sample with several perovskite PV cells was incorporated to one end of the light guide matching the part of one cell area with the guide thickness. To measure the J–V under green illumination a neodymium-doped yttrium aluminum garnet 532 nm laser (Coherent Compass) was employed and its light was polarized. Enough s-polarized light was inserted so the J_{sc} current measured was similar to the one obtained under direct illumination. Then, the same intensity of p-polarized light was inserted to measure the J–V curve under this condition. To measure the current ratio, the CPS sources were employed and the current under short-circuit condition was measured for the same intensity of s- and p-polarized light.

Optical Simulation of the Perovskite PV Cells: PV cell parameters are calculated using full-wave generalized detailed balance model based on transfer matrix method for s- and p-polarizations for normal and oblique light incidence, followed by optical power dissipation calculation. Details on the optical model can be found in ref. [38].

Supporting Information

Supporting Information is available from the Wiley Online Library or from the author.

Acknowledgements

Conflict of Interest

The authors declare no conflict of interest.

Data Availability Statement

The data that support the findings of this study are available from the corresponding author upon reasonable request.

[1] M. F. Weber, C. A. Stover, L. R. Gilbert, T. J. Nevitt, A. J. Ouderkirk, *Science* **2000**, *287*, 2451.

[2] X. Yang, Y. Yan, G. Jin, *Opt. Express* **2005**, *13*, 8349.

[3] M. Suzuki, *J. Soc. Inf. Disp.* **1999**, *7*, 157.

[4] Y. Li, S. T. Wu, T. X. Wu, *J. Disp. Technol.* **2009**, *5*, 335.

[5] K. W. Chien, H. P. D. Shieh, *App. Opt.* **2004**, *43*, 1830.

[6] M. Y. Yu, B. W. Lee, J. H. Lee, J. H. Ko, *J. Opt. Soc. Korea* **2009**, *13*, 256.

[7] R. Zhu, A. Kumar, Y. Yang, *Adv. Mater.* **2011**, *23*, 4193.

[8] B. Park, Y. H. Huh, J. C. Shin, *Sol. Energy Mater. Sol. Cells* **2011**, *95*, 3543.

[9] A. Menéndez-Velázquez, C. L. Mulder, N. J. Thompson, T. L. Andrew, P. D. Reusswig, C. Rotschild, M. A. Baldo, *Energy Environ. Sci.* **2013**, *6*, 72.

[10] S. D. Stranks, G. E. Eperon, G. Grancini, C. Menelaou, M. J. P. Alcocer, T. Leijtens, L. M. Herz, A. Petrozza, H. J. Snaith, *Science* **2013**, *342*, 341.

[11] D. Luo, R. Su, W. Zhang, Q. Gong, R. Zhu, *Nat. Rev. Mater.* **2020**, *5*, 44.

[12] Q. Lin, A. Armin, R. C. R. Nagiri, P. L. Burn, P. Meredith, *Nat. Photonics* **2015**, *9*, 106.

[13] M. Stolterfoht, C. M. Wolff, J. A. Márquez, S. Zhang, C. J. Hages, D. Rothhardt, S. Albrecht, P. L. Burn, P. Meredith, T. Unold, D. Neher, *Nat. Energy* **2018**, *3*, 847.

[14] W. Tress, *Adv. Energy Mater.* **2017**, *7*, 1602358.

[15] C. M. Wolff, P. Caprioglio, M. Stolterfoht, D. Neher, *Adv. Mater.* **2019**, *31*, 1902762.

[16] J. H. Noh, S. H. Im, J. H. Heo, T. N. Mandal, S. Il Seok, *Nano Lett.* **2013**, *13*, 1764.

[17] S. Gharibzadeh, I. M. Hossain, P. Fassl, B. A. Nejand, T. Abzieher, M. Schultes, E. Ahlswede, P. Jackson, M. Powalla, S. Schäfer, M. Rienäcker, T. Wietler, R. Peibst, U. Lemmer, B. S. Richards, U. W. Paetzold, *Adv. Funct. Mater.* **2020**, *30*, 1909919.

[18] S. H. Turren-Cruz, A. Hagfeldt, M. Saliba, *Science* **2018**, *362*, 449.

[19] Z. Yang, A. Rajagopal, S. B. Jo, C. C. Chueh, S. Williams, C. C. Huang, J. K. Katahara, H. W. Hillhouse, A. K. Y. Jen, *Nano Lett.* **2016**, *16*, 7739.

[20] M. T. Hörantner, T. Leijtens, M. E. Ziffer, G. E. Eperon, M. G. Christoforo, M. D. McGehee, H. J. Snaith, *ACS Energy Lett.* **2017**, *2*, 2506.

[21] C. Chen, Z. Song, C. Xiao, D. Zhao, N. Shrestha, C. Li, G. Yang, F. Yao, X. Zheng, R. J. Ellingson, C. S. Jiang, M. Al-Jassim, K. Zhu, G. Fang, Y. Yan, *Nano Energy* **2019**, *61*, 141.

[22] Z. Song, C. Chen, C. Li, R. Awni A, D. Zhao, Y. Yan, *Semicond. Sci. Technol.* **2019**, *34*, 093001.

[23] C. Bi, Y. Yuan, Y. Fang, J. Huang, *Adv. Energy Mater.* **2015**, *5*, 1401616.

[24] C. G. Ferreira, G. Martínez-Denegri, M. Kramarenko, J. Toudert, J. Martorell, *Adv. Photonics Res.* **2021**, *2*, 2100077.

[25] G. Martínez-Denegri, S. Colodrero, Q. Liu, J. Toudert, G. Kozyreff, J. Martorell, *Adv. Opt. Mater.* **2019**, *7*, 1900018.

[26] M. Barhoum, J. M. Morrill, D. Riassetto, M. H. Bartl, *Chem. Mater.* **2011**, *23*, 5177.

[27] A. L. Thomann, C. Vahlas, L. Aloui, D. Samelor, A. Caillard, N. Shaharil, R. Blanc, E. Millon, *Chem. Vap. Deposition* **2011**, *17*, 366.

[28] K. E. Elers, T. Blomberg, M. Peussa, B. Aitchison, S. Haukka, S. Marcus, *Chem. Vap. Deposition* **2006**, *12*, 13.

[29] D. M. Mattox, in *Handbook of Physical Vapor Deposition (PVD) Processing*, William Andrew, Norwich, New York **2010**, pp. 333–398.

[30] C. Chen, S. Zheng, H. Song, *Chem. Soc. Rev.* **2021**, *50*, 7250.

[31] N. G. Park, *ACS Energy Lett.* **2019**, *4*, 2983.

[32] S. Gozalzadeh, F. Nasirpouri, S. il Seok, *Sci. Rep.* **2021**, *11*, 18561.

[33] A. Y. Alsalloum, B. Turedi, K. Almasabi, X. Zheng, R. Naphade, S. D. Stranks, O. F. Mohammed, O. M. Bakr, *Energy Environ. Sci.* **2021**, *14*, 2263.

[34] S. Gharibzadeh, P. Fassl, I. M. Hossain, P. Rohrbeck, M. Frericks, M. Schmidt, T. Duong, M. R. Khan, T. Abzieher, B. A. Nejand, F. Schackmar, O. Almora, T. Feeney, R. Singh, D. Fuchs, U. Lemmer, J. P. Hofmann, S. A. L. Weber, U. W. Paetzold, *Energy Environ. Sci.* **2021**, *14*, 5875.

[35] D. Kiermasch, L. Gil-Escrig, H. J. Bolink, K. Tvingstedt, *Joule* **2019**, *3*, 16.

[36] J. Wang, G. Huang, Y. Mei, *Chem. Vap. Deposition* **2014**, *20*, 103.

[37] J. Alami, S. Bolz, K. Sarakinos, *J. Alloys Compd.* **2009**, *483*, 530.

[38] M. Kramarenko, C. G. Ferreira, G. Martínez-Denegri, C. Sansierra, J. Toudert, J. Martorell, *Sol. RRL* **2020**, *4*, 1900554.